

Mathematical modelling of scanner-specific bowtie filters for Monte Carlo CT dosimetry

This content has been downloaded from IOPscience. Please scroll down to see the full text.

2017 Phys. Med. Biol. 62 781

(<http://iopscience.iop.org/0031-9155/62/3/781>)

View [the table of contents for this issue](#), or go to the [journal homepage](#) for more

Download details:

IP Address: 156.145.140.22

This content was downloaded on 22/02/2017 at 21:22

Please note that [terms and conditions apply](#).

You may also be interested in:

[The development, validation and application of a MDCT scanner model](#)

J Gu, B Bednarz, P F Caracappa et al.

[Organ and effective doses in newborn patients during MSCT](#)

Robert J Staton, Choonik Lee, Choonsik Lee et al.

[A Monte Carlo based method to estimate radiation dose from multidetector CT \(MDCT\)](#)

J J DeMarco, C H Cagnon, D D Cody et al.

[Investigation of practical approaches to evaluating cumulative dose for cone beam computed tomography \(CBCT\) from standard CT dosimetry measurements: a Monte Carlo study](#)

Abdullah Abuhaimeed, Colin J Martin, Marimuthu Sankaralingam et al.

[Development of 1-year-old computational phantom and calculation of organ doses during CT scans using Monte Carlo simulation](#)

Yuxi Pan, Rui Qiu, Linfeng Gao et al.

[A Monte Carlo-based method to estimate radiation dose from spiral CT](#)

G Jarry, J J DeMarco, U Beifuss et al.

[Entrance surface air kerma and energy imparted in CT](#)

P Avilés Lucas, D R Dance, I A Castellano et al.

[A measurement-based generalized source model for Monte Carlo dose simulations of CT scans](#)

Xin Ming, Yuanming Feng, Ransheng Liu et al.

[A practical approach to estimate the weighted CT dose index over an infinite integration length](#)

Xinhua Li, Da Zhang and Bob Liu

Mathematical modelling of scanner-specific bowtie filters for Monte Carlo CT dosimetry

R Kramer¹, V F Cassola¹, M E A Andrade¹, M W C de Araújo¹,
D J Brenner² and H J Khoury¹

¹ Department of Nuclear Energy, Federal University of Pernambuco, Avenida Prof Luiz Freire, 1000, CEP 50740-540, Recife, Brazil

² Center for Radiological Research, Columbia University Medical Centre, New York, NY, USA

E-mail: rkramer@uol.com.br

Received 21 September 2015, revised 24 November 2016

Accepted for publication 12 December 2016

Published 10 January 2017



CrossMark

Abstract

The purpose of bowtie filters in CT scanners is to homogenize the x-ray intensity measured by the detectors in order to improve the image quality and at the same time to reduce the dose to the patient because of the preferential filtering near the periphery of the fan beam. For CT dosimetry, especially for Monte Carlo calculations of organ and tissue absorbed doses to patients, it is important to take the effect of bowtie filters into account. However, material composition and dimensions of these filters are proprietary. Consequently, a method for bowtie filter simulation independent of access to proprietary data and/or to a specific scanner would be of interest to many researchers involved in CT dosimetry. This study presents such a method based on the weighted computer tomography dose index, $CTDI_w$, defined in two cylindrical PMMA phantoms of 16 cm and 32 cm diameter. With an EGSnrc-based Monte Carlo (MC) code, ratios $CTDI_w/CTDI_{100,a}$ were calculated for a specific CT scanner using PMMA bowtie filter models based on sigmoid Boltzmann functions combined with a scanner filter factor (SFF) which is modified during calculations until the calculated MC $CTDI_w/CTDI_{100,a}$ matches ratios $CTDI_w/CTDI_{100,a}$, determined by measurements or found in publications for that specific scanner. Once the scanner-specific value for an SFF has been found, the bowtie filter algorithm can be used in any MC code to perform CT dosimetry for that specific scanner. The bowtie filter model proposed here was validated for $CTDI_w/CTDI_{100,a}$ considering 11 different CT scanners and for $CTDI_{100,c}$, $CTDI_{100,p}$ and their ratio considering 4 different CT scanners. Additionally, comparisons were made for lateral dose profiles free in air and using computational anthropomorphic phantoms. $CTDI_w/CTDI_{100,a}$ determined with this new method agreed on average

within 0.89% (max. 3.4%) and 1.64% (max. 4.5%) with corresponding data published by CTDosimetry (www.impactscan.org) for the CTDI HEAD and BODY phantoms, respectively. Comparison with results calculated using proprietary data for the PHILIPS Brilliance 64 scanner showed agreement on average within 2.5% (max. 5.8%) and with data measured for that scanner within 2.1% (max. 3.7%). Ratios of $CTDI_{100,c}/CTDI_{100,p}$ for this study and corresponding data published by CTDosimetry (www.impactscan.org) agree on average within about 11% (max. 28.6%). Lateral dose profiles calculated with the proposed bowtie filter and with proprietary data agreed within 2% (max. 5.9%), and both calculated data agreed within 5.4% (max. 11.2%) with measured results. Application of the proposed bowtie filter and of the exactly modelled filter to human phantom Monte Carlo calculations show agreement on the average within less than 5% (max. 7.9%) for organ and tissue absorbed doses.

Keywords: CT dosimetry, bowtie filter, exposure to patients

(Some figures may appear in colour only in the online journal)

1. Introduction

Apart from flat filters mostly made of aluminium, computerized tomography (CT) scanners also have beam-shaping filters made of metal and/or plastic material, which frequently are called bowtie filters because of their characteristic shape. The function of flat filters is to remove the low-energy photons from the x-ray spectrum because they do not contribute to the signal at the detector but only to organ and tissue absorbed doses (=dose) to the patient; the purpose of bowtie filters is to homogenize the x-ray intensity measured by the detectors in order to improve the image quality and at the same time to reduce the dose to the patient because of the preferential filtering near the periphery of the fan beam.

Experimental studies of scatter and patient dose reduction as a function of bowtie filter properties have been published by Graham *et al* (2007) and Mail *et al* (2009), while calculation methods (analytical or Monte Carlo) have been used by Tkaczyk *et al* (2004), Bootsma *et al* (2011) and Kontson and Jennings (2015) for the investigation of the same problem. The studies confirm the benefits of lower patient dose and improved image quality but at the expense of reduced contrast-to-noise ratio at the edge of the image.

As far as doses to patients from medical procedures are concerned, CT became the main contributor for mainly two reasons: First, compared to conventional radiography a CT examination usually causes higher exposure of the patient (Bauhs *et al* 2008). Second, the number of CT examinations per year is rising rapidly. In the US, the number of CT examinations went from 3.6 million in 1980 to 72 million in 2007 (NCRP 2009), for example. Similar trends can be observed in many other countries. Consequently, in recent years radiation risk considerations (Brenner *et al* 2001, Brenner and Hall 2007) and the determination of organ and tissue absorbed doses to patients from exposure to CT examinations became a major issue in the radiation protection community. Corresponding investigations typically use Monte Carlo codes coupled to human phantoms, simulating the exposure to the patient straightforward (DeMarco *et al* 2007, Liu *et al* 2010, Li *et al* 2011, Lee *et al* 2012, McMillan *et al* 2014). In order to do this, the properties and the movement of the CT x-ray tube must be simulated properly, including x-ray spectra, flat filters, as well as the material composition and the shape of the bowtie filter, which are normally proprietary.

Turner *et al* (2009) presented an ‘equivalent’ source model which consists of an energy spectrum and filtration description based on measurements of the half value layers (HVL₁ and HVL₂) and the bowtie filter profile (=exposure values across the fan beam) for the CT scanner of interest. The ‘equivalent’ bowtie filter attenuates the ‘equivalent’ spectrum in a similar fashion as the actual filtration attenuates the actual x-ray beam. This ‘equivalent’ source model can be used in Monte Carlo CT simulations independently from proprietary data to be provided by the manufacturer.

Using a probe placed at the edge of a scanner’s field of view, Boone (2010) and McKenney *et al* (2011) developed a method ‘for characterization of bowtie relative attenuation (COBRA)’ based on filtered and unfiltered data sets. The COBRA method allows for the computation of the angle-dependent bowtie filter attenuation and of the thickness of the filter, thus providing with only little expenditure on measurements the information necessary for Monte Carlo CT dosimetry.

Bow tie profiles using a real time dosimeter and applying the COBRA method were published by Whiting *et al* (2014) for five CT scanners made by three manufacturers. Relative errors in the profiles were found to be less than 5% and a comparison with a direct measurement technique on one system produced agreement with a relative error of 2%–6%. Additionally, Whiting *et al* (2015) described the construction of an inexpensive aperture, which is used to expose radiochromic film in a rotating CT gantry. Based on the measured data, bow tie profiles were determined and compared with other existing methods. This radiochromic film method can measure radiation exposure with a precision of 6% root-mean-square relative error. This error is up to 25% when compared with other techniques.

A scintillator based x-ray detector was used by Li *et al* (2015a) to measure radiation exposure across a scan field-of-view. Bowtie attenuation was calculated as ratio between exposure measurements with and without bow tie filter. The bow tie profiles were then used in Monte Carlo calculations using the images of a human cadaver. The same cadaver was also used for measurements of organ doses. The median difference between calculated and measured organ doses was found to be 8.9%.

Based on non-disclosure agreements, some research groups obtained bowtie filter specifications for one or two scanner from a specific manufacturer. However, there are many other scanners in use all over the world, and not every research group who wants to simulate CT examinations succeeds to obtain the necessary bowtie filter information. Consequently, a method for bowtie filter simulation independent of proprietary data and easy to implement would be in the interest of many researchers involved in Monte Carlo CT dosimetry.

Therefore, we suggest a mathematical model of bowtie filter design based on the Monte Carlo calculated weighted computer tomography dose index, CTDI_w, for a specific scanner, a method developed at the Federal University of Pernambuco (UFPE = Universidade Federal de Pernambuco). If the calculated CTDI_w/CTDI_{100,a} agrees with corresponding data measured with that scanner or calculated using proprietary data for the bowtie filter of that scanner or taken from the scanner manual or from scientific publications, then this virtual bowtie filter model is considered to represent the real bowtie filter properly and can be used for Monte Carlo calculation in CT dosimetry without having to receive proprietary data from CT manufacturers.

This approach was also motivated by the idea of a ‘perfect filter’ described by Atherton (1993) and Huda and Atherton (1995) as ‘an acrylic perfect filter, whose shape gives a constant x-ray beam path length through the scanned (acrylic) cylinder, simulated the case of constant transmission of primary x-ray photons through the phantom’. Different from the concept described by Huda and Atherton, our proposed ‘perfect bowtie filter’ would produce equal dose in the centre and at the periphery of a CTDI phantom.

2. Materials and methods

2.1. Quantities in CT dosimetry

The computed tomography dose index (CTDI) has served as a standard dose descriptor in CT dosimetry since the 1980s (Jucius and Kambic 1977, Shope *et al* 1991) and, since the availability of standardized 100 mm length pencil ionization chambers, it is defined as:

$$\text{CTDI}_{100} = \frac{1}{nT} \int_{-50\text{mm}}^{50\text{mm}} D(z) dz$$

where n represents the number of slices (rotations), T the slice thickness (collimation) and $D(z)$ the dose profile along the axis of rotation over a distance of 100 mm. In this investigation, D represents the air kerma, $n = 1$ and $T = 1$ cm.

Additionally, two cylindrical CTDI phantoms made of polymethyl metacrylate (PMMA) with 15 cm length have been defined, one with 16 cm diameter, called HEAD phantom, the other with 32 cm diameter, called BODY phantom. Both phantoms have five cylindrical holes parallel to the axis with 1 cm diameter and 10 cm lengths, one being located in the centre and four distributed along the circular periphery at 0° (NORTH), 90° (WEST), 180° (SOUTH) and 270° (EAST).

CTDI₁₀₀ can be measured in air, CTDI_{100,a}, or inside the CTDI phantoms parallel to the axis of rotation (McNitt-Gray 2002). The weighted index, CTDI_w, is a dose index which represents a weighted average of the dose distribution within the cylindrical phantom and is defined as:

$$\text{CTDI}_w = (1/3) \text{CTDI}_{100,c} + (2/3) \text{CTDI}_{100,p},$$

where CTDI_{100,c} represents the CTDI₁₀₀ in the centre hole of the CTDI phantom, while CTDI_{100,p} represents the average CTDI₁₀₀ for the four peripheral holes.

For helical scans one can define a volumetric index, CTDI_{vol}, given by

$$\text{CTDI}_{\text{vol}} = \text{CTDI}_w / \text{pitch}.$$

Pitch is the table increment per rotation of the CT scanner divided by the collimation.

2.2. Monte Carlo modelling of bowtie filter and CTDI

2.2.1. Monte Carlo calculation. Based on an EGSnrc computer programme for simulating exposure from a point source rotating around the human body length axis (Kramer *et al* 2010), a Monte Carlo code representing a CT x-ray tube rotating around cylindrical CTDI phantoms with 0.5 mm × 0.5 mm × 1 mm voxel size has been developed, by replacing the human phantom with the two CTDI phantoms shown in figures 1 and 2. Inside the 1 cm diameter holes, the first millimetre represents the PMMA wall of the ionization chamber, thus the cylindrical air volume has a diameter of 8 mm and 10 cm length.

Figure 3 (left) shows the chamber walls around the holes in the phantom cross-section. CTDI₁₀₀ was calculated in air and in the phantoms for one single axial rotation of the x-ray tube in the x - y plane around the centre of the CTDI phantom, with 1 cm collimation defined in the centre of rotation.

During Monte Carlo calculations, cut-off energies were set to 2 keV for photons and 150 keV for electrons, thus providing an estimate of kerma rather than absorbed dose. CT scanners, usually operating with tube potential less than 150 kVp, would liberate secondary electrons in PMMA with ranges of 0.24 mm or less (NIST 2015). The contribution of these electrons to the dose distribution in PMMA can therefore be neglected.

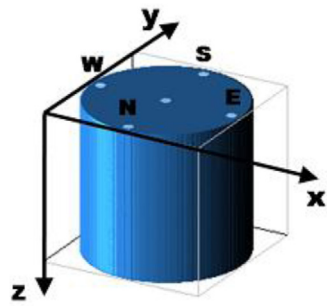


Figure 1. CTDI HEAD phantom.

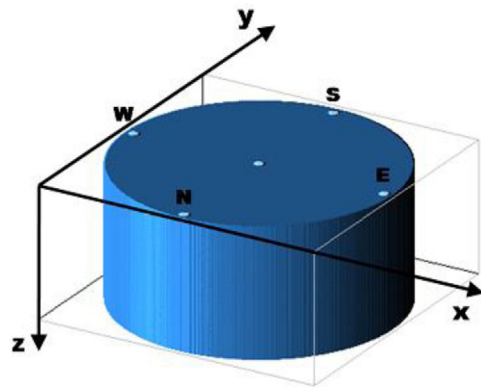


Figure 2. CTDI BODY phantom.

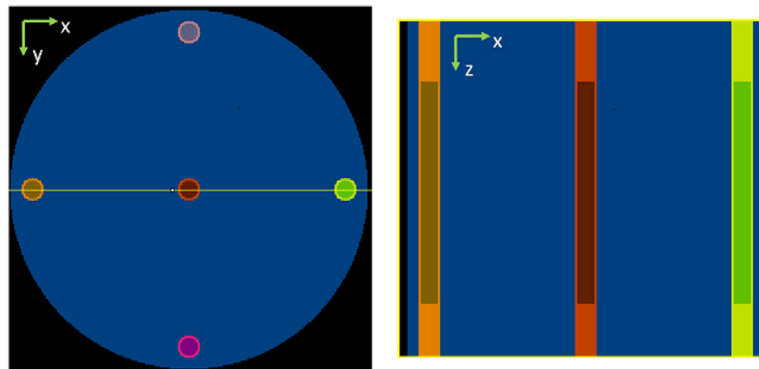


Figure 3. CTDI phantom: frontal and lateral view of the holes, which consist of cylindrical air volumes surrounded by a PMMA wall of 1 mm thickness representing the pencil ionization chamber.

Monte Carlo calculation in the 10 cm air holes would be very time consuming in order to arrive at a statistical error of about 1–2%, because of the low density of air, which makes photon interactions less frequent, and, at the same time, because of the much greater electron range compared to PMMA. Applying a method already used by Boone (2007) and Li *et al* (2015b), photon interactions were simulated assuming the holes are filled with PMMA and

the results were then transformed into air kerma using ratios between the mass-energy absorption coefficients (MEAC) of air and PMMA. Thereby, it is possible to do a calculation with 20 million source photons in about 15 minutes on a desktop computer with a Pentium CORE i7 processor achieving a statistical error of about 1%, also maintaining the above mentioned cut-off energies. A detailed description of this method is given in the annex to this paper.

Apart from the bowtie filters, also scanner-specific x-ray spectra including flat filters are proprietary. Therefore, using the IPREM Report 78 (Cranley *et al* 1997) a file with 49 x-ray spectra was generated containing tube potentials between 80 and 140 kVp, with filtrations between 4 and 10 mm Al, for a 7° anode angle. CTDI₁₀₀ in the centre and the peripheral holes were calculated in terms of air kerma as described in the previous paragraph. Additionally, the Monte Carlo code tallies the source photons in the field centre for an area equivalent to the size of the pencil chamber to calculate the air kerma at the iso-centre free in air for the purpose of normalization, using the fluence-to-air kerma conversion coefficients given in ICRP 74 (ICRP 1996). The Monte Carlo code calculates CTDI quantities normalized to fluence and air kerma at the centre of rotation, as well as to the time-current product. Figure 4 shows the exposure geometry without bowtie filter, with a fan beam angle of 56°, where DSI is the distance between source and the iso-centre of rotation and R the radius of the cylindrical CTDI phantom. Values for the DSI and the fan beam angle can usually be found in the scanner manual.

For the Monte Carlo calculations of the lateral dose profiles free in air, the exposure geometry was changed: Additionally to the central hole, seven holes with PMMA walls with 2 cm intervals between them were introduced laterally according to figure 5. The space around them was considered to be air. Again, air kerma inside the eight holes was determined using the MEA coefficient method described above. While the measurement was carried out with one pencil ionization chamber located in eight different positions, the Monte Carlo calculation was done in all eight PMMA holes at the same time.

2.2.2. Bowtie filter attenuation. In Monte Carlo calculations, x-ray spectra to be used for selecting initial photon energies, typically already include the effect of the flat filter, but not of the bowtie filter. Simulating photon interactions in the bowtie filter is quite time consuming because many scattered photons leave the filter without having any chance to reach the phantom. Therefore, the attenuation by the bowtie filter is taken into account by assigning a weight W to every photon leaving the x-ray source with initial energy E at an angle θ , given by

$$W(E, \theta) = \exp[-\mu(E) \cdot t(\theta)], \quad (1)$$

where E is the start energy of the photon, $\mu(E)$ represents the linear attenuation coefficient (NIST 2015) of the filter material for energy E , and $t(\theta)$ the trajectory of a primary photon through the bowtie filter (=thickness) as a function of the emission angle θ , which is the angle between the photon direction and the central ray of the fan beam. $W(E, \theta)$ is thus the probability that the photon was transmitted through the filter. It has been shown that dose to human phantoms calculated by this simple attenuation method agreed within a margin of 1% with corresponding results from explicit Monte Carlo calculations (Jones and Shrimpton 1991).

The primary function of a bowtie filter is to homogenize the photon flux at the detectors by attenuating the fan beam more at its periphery; this is to compensate for less attenuation by peripheral regions of the patient's body. Originally intended to improve the image quality, bowtie filters also have a beneficial side effect, namely the reduction of dose to the patient exactly in those peripheral regions of the body (Graham *et al* 2007, Mail *et al* 2009). Consequently, the dose distribution across the body becomes more homogeneous—although not completely because of the different tissue densities and the elliptical cross-section of the supine human body. One can expect to improve the homogeneity of the dose distribution if the

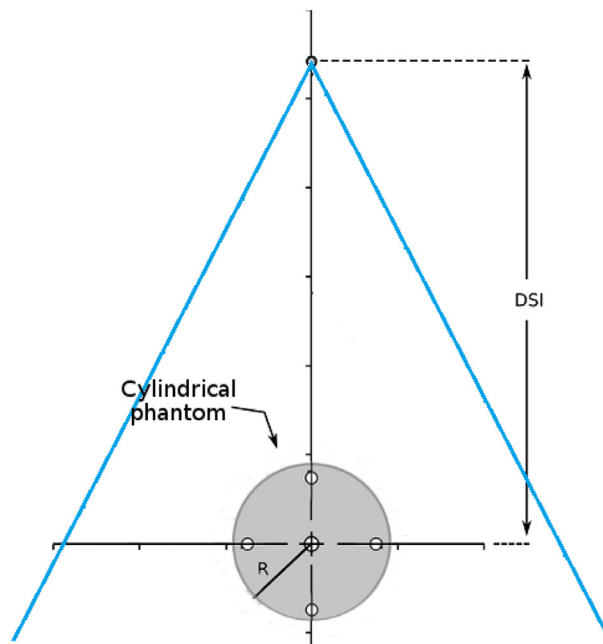


Figure 4. CT exposure geometry for a cylindrical CTDI phantom (without bowtie filter).

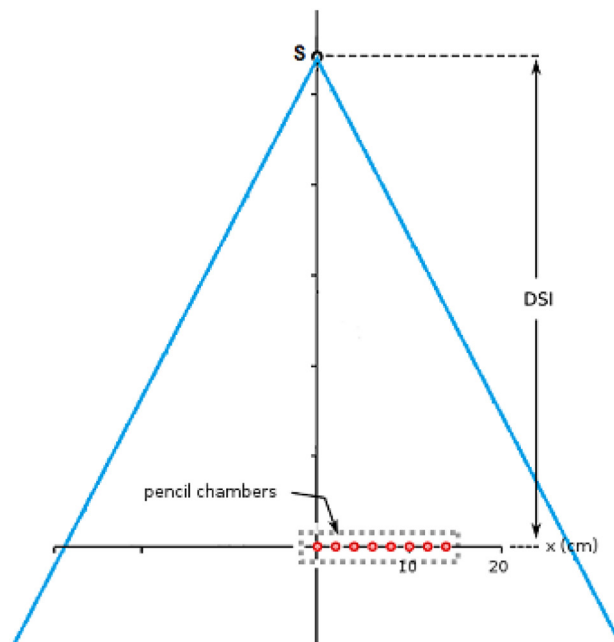


Figure 5. CT exposure geometry for eight holes with PMMA walls (=pencil ionization chambers) free in air with 2 cm intervals between them (bowtie filter not shown) for lateral profile calculations.

Table 1. CTDI₁₀₀ data for four CT scanners and four tube potentials extracted from CTDosimetry (www.impactscan.org). Columns C/P added by the authors of this study.

kV	Scanner	CTDI (Head, mGy/100 mAs)				CTDI (Body, mGy/100 mAs)			
		Air	Centre	Perip	C/P	Air	Centre	Perip	C/P
80	GE Lightspeed Ultra	14.2	7.7	8.2	0.94	10.5	1.8	4.5	0.40
100		23.8	14.5	14.7	0.99	18.9	3.9	8.5	0.46
120		35.0	22.5	22.3	1.01	29.0	7.0	13.8	0.50
140		47.4	31.6	30.9	1.02	40.5	9.9	18.9	0.52
80	Philips Brilliance 64 or 40	7.0	4.6	5.4	0.85	7.0	1.3	3.0	0.43
120		21.5	15.7	16.8	0.93	21.5	5.1	10.0	0.51
140		31.0	22.9	24.8	0.92	31.0	7.9	14.9	0.53
80	Siemens Definition AS	5.7	3.3	3.6	0.93	5.7	0.9	2.0	0.44
100		10.5	6.7	7.1	0.95	10.4	1.9	3.9	0.49
120		16.9	11.3	11.8	0.96	16.9	3.5	6.6	0.53
140		24.3	16.6	17.3	0.96	24.3	5.5	9.7	0.56
80	Toshiba Aquilion 16	15.9	8.3	10.1	0.82	21.9	2.4	6.6	0.36
100		25.3	15.7	17.3	0.90	33.2	4.8	11.7	0.41
120		36.2	24.5	26.6	0.92	45.8	8.0	17.4	0.46
135		45.4	32.5	35.0	0.93	56.1	11.0	23.1	0.48

human body is replaced with a homogeneous cylindrical phantom with an appropriate diameter, and if phantom and bowtie filter are made of the same material: Using a ‘perfect bowtie filter’ made of PMMA one would measure equal air kerma in the centre and at the periphery of a CTDI phantom, for example.

CTDosimetry 1.0.4, available at www.impactscan.org, is a CT Patient Dosimetry Calculator which contains CTDI₁₀₀ data for almost 70 CT scanners from various manufacturers. Extracted from CTDosimetry, table 1 shows CTDI_{100,a} (Air), CTDI_{100,c} (Centre) and CTDI_{100,p} (Perip) in mGy/100 mAs as a function of the tube potential for the HEAD and the BODY PMMA phantoms for four different CT scanners and tube potentials. CTDI_{100,a}/100 mAs refers to the centre of rotation in air, i.e. this quantity can be considered as the output of the x-ray tube. The C/P columns, added by the authors of this study, show CTDI₁₀₀ ratios between Centre and Periphery for the two phantoms, respectively. As one can see, most HEAD phantom ratios C/P are close to 1.0, which indicates that in these scanners and at these tube potentials the bowtie filters succeed to create an almost homogeneous dose distribution, the one caused by a ‘perfect filter’. More or less filtration at the periphery is reflected by the value of the C/P ratio depending if it is greater or smaller than 1.0, respectively.

For the larger BODY phantom C/P ratios are mostly close to 0.5. Consequently, for Monte Carlo CT dosimetry one has to find a general mathematical model for bowtie filters which produces ratios CTDI_{100,c}/CTDI_{100,p} = 1 for the CTDI HEAD phantom and 0.5 for the CTDI BODY phantom. Specific scanner considerations would then be added later to the basic model through a correction factor.

2.3. Basic bowtie filters

Figure 6 shows the exposure scenario with the basic bowtie filter, the CTDI HEAD PMMA phantom with radius R , in a distance source-to-iso-centre (DSI) of 54 cm and the trajectory of a photon leaving the source at an angle θ , travelling a distance $t(\theta)$ and $P(\theta)$ through the bowtie filter and the cylindrical phantom, respectively. $P(\theta)$ and $t(\theta)$ are complementary, i.e. that for

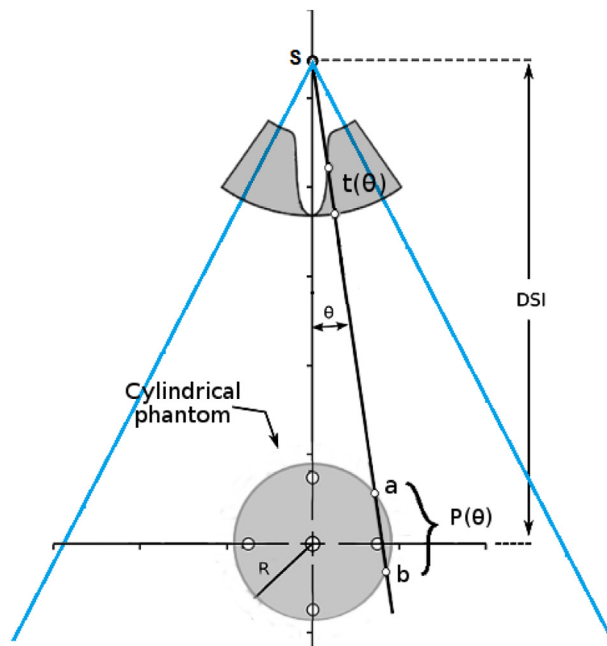


Figure 6. CT exposure geometry for the CTDI HEAD phantom and the basic bowtie filter made of PMMA.

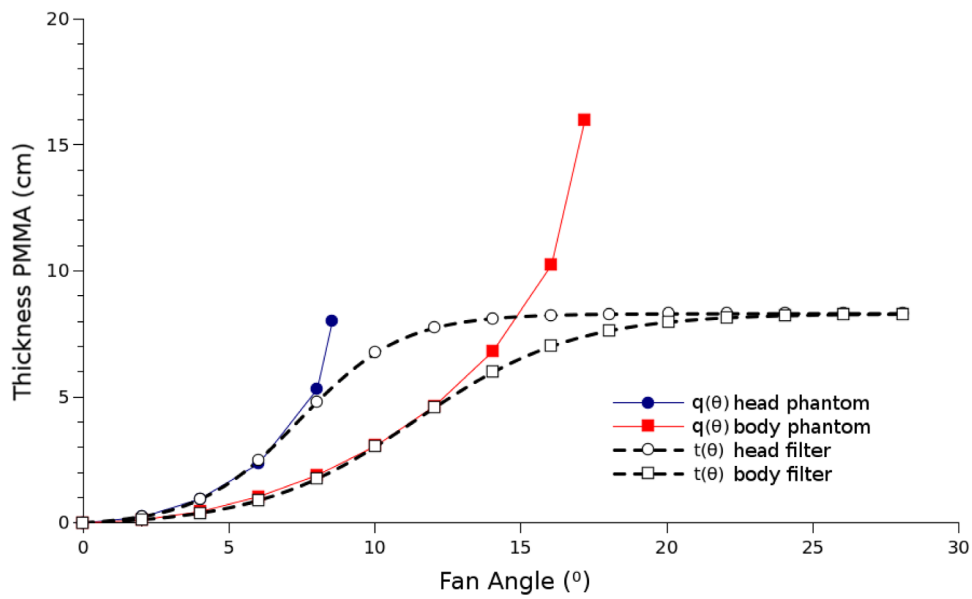


Figure 7. PMMA filter thickness as function of the fan angle: first approximation bowtie models $q(\theta)$ for the HEAD and the BODY phantoms for $\theta < \theta_{Limit}$. Mathematical models $t(\theta)$ for the final bowtie filters covering the whole angular range of the fan beam. After calculating bowtie filter thicknesses for various fan angles, the software QtiPlot was used to fit a curve through the calculated data points.

$\theta = 0$, $P(\theta) = 2R$ and $t(\theta) = 0$, while for $\theta = \theta_{\text{Limit}}$, $P(\theta_{\text{Limit}}) = 0$ and $t(\theta_{\text{Limit}}) = t_{\text{Limit}}$, with θ_{Limit} being the angle for which a photon does not enter the phantom anymore. Consequently, for $\theta > \theta_{\text{Limit}}$, $t(\theta)$ remains constant. The material of the bowtie filter is assumed also to be PMMA and the fan angle is 56° .

The length of the photon's trajectory through the cylindrical phantom, $P(\theta)$, is given by

$$P(\theta) = 2 \sqrt{R^2 - \text{DSI}^2 * \sin^2(\theta)}. \quad (2)$$

For the air kerma to be equal in the centre and at the periphery of the 8 cm radius HEAD phantom, the basic bowtie filter should have a thickness of $t(\theta) = 0$ for $\theta = 0$, and of $t(\theta) = 8$ cm for $\theta = \theta_{\text{Limit}}$. Therefore, in a first approximation the mathematical model for the basic bowtie filter satisfying these conditions can be defined as

$$q(\theta) = R - P(\theta)/2 = R - \sqrt{R^2 - \text{DSI}^2 * \sin^2(\theta)} \quad (3)$$

shown in figure 7 as blue curve with circles for the HEAD phantom, which represents the bowtie filter thickness as a function of the photon's angle with the central ray of the fan beam. $q(\theta)$ covers the angular range up to θ_{Limit} , which is about 8.5° for the HEAD phantom. In order to combine the angular dependent part ($\theta < \theta_{\text{Limit}}$) with the constant part ($\theta > \theta_{\text{Limit}}$) of the bowtie filter thickness $t(\theta)$ in a continuous manner, a sigmoid Boltzmann function given by

$$t(\theta) = (a - b)/(1.0 + \exp((\theta * AC - c)/d)) + b, \quad (4)$$

was chosen, where the coefficients a , b , c and d have the values given in table 2 for the HEAD phantom filter in the last column. Initially, $t(\theta)$, shown in figure 7 as the black curve with circles, follows the function $q(\theta)$ until approximately $\theta = 7.5^\circ$. Then, the function smoothly approaches the constant value of 8 cm. Similar considerations apply to the bowtie filter for the BODY phantom, but lead to different values for the coefficients because its diameter is 32 cm instead of 16 cm. Corresponding values for the BODY coefficients are also shown in table 2. Corresponding curves are shown for the BODY phantom in figure 7 in red and with squares. Here, the Boltzmann function follows $q(\theta)$ up to an angle θ of about 12° before starting to approach the 8 cm thickness smoothly. AC in equation (4) takes DSIs different from 54 cm into account given by $AC = \text{atan}(8/54)/\text{atan}(8/\text{DSI})$ for the HEAD filter, or $AC = \text{atan}(16/54)/\text{atan}(16/\text{DSI})$ for the BODY filter.

2.4. Scanner-specific bowtie filters

Once the basic bowtie filters have been defined, one can now think about adapting them to specific CT scanners, whose CTDI_w are known, like those published by CT Dosimetry, for example, or were measured for a specific scanner. Therefore a scanner filter factor (SFF) is introduced into the equation for the weight W , which now becomes

$$W(E, \theta, \text{SFF}) = \exp[-\mu(E) \cdot t(\theta) \cdot \text{SFF}]. \quad (5)$$

Using scanner-specific data available at www.impactscan.org, in particular the DSI, Monte Carlo calculations were made, varying the value of SFF until the calculated $\text{CTDI}_w/\text{CTDI}_{100,a}$ agreed with the known $\text{CTDI}_w/\text{CTDI}_{100,a}$ for that particular scanner. Once the SFF has been determined, the Monte Carlo calculation using a human phantom, for example, can be executed.

For each source photon i , a subroutine is called which calculates $W(E_i, \theta_i, \text{SFF})$ as a function of the CTDI phantom diameter, the initial photon energy E_i , the emission angle of the photon θ_i , the DSI and the SFF. To calculate the dose (=air kerma) in a voxel of the cylindrical

Table 2. Coefficients for the sigmoid Boltzmann functions which describe the basic bowtie filters.

	Body filter	Head filter
A	8.301 5550 (cm)	8.299 9360 (cm)
B	−0.122 8647 (cm)	−0.120 4692 (cm)
c	0.199 2510	0.129 4980
d	−0.047 2935	−0.030 6382

Table 3. Dose per air kerma at the iso-centre in the air volumes of the CTDI phantoms without bowtie filter and with basic bowtie filters. C.V. = coefficient of variance (statistical error).

Basic Bowtie	CTDI HEAD phantom				CTDI BODY phantom	
	SFF = 0, W = 1		SFF = 1, W = exp[−μ(E) · t(θ)]		Dose/air kerma (Gy/Gy)	C.V. (%)
	Dose/air kerma (Gy/Gy)	C.V. (%)	Dose/air kerma (Gy/Gy)	C.V. (%)		
Air volume						
Centre	0.0763	0.64	0.0692	0.65	0.0216	1.64
North	0.0938	0.58	0.0672	0.60	0.0442	1.01
East	0.0938	0.58	0.0680	0.60	0.0448	1.02
South	0.0927	0.58	0.0667	0.60	0.0450	1.01
West	0.0937	0.58	0.0684	0.60	0.0455	0.99

holes during the Monte Carlo calculations, the energy deposited per photon, EDEP, has to be weighted with the function $W(E_i, \theta_i, \text{SFF})$ and summed for all initial photon energies E_i and angles θ_i :

$$\text{SEDEP} = \sum_i \text{EDEP} \cdot W(E_i, \theta_i, \text{SFF}), \quad (6)$$

which is the total energy deposited per voxel. The sum of the energy deposited in all voxels of the cylindrical holes is then used to calculate the dose in PMMA.

For the conversion of PMMA dose to air dose, first the ratio of the MEAC between air and PMMA according to column 4 of table A1 is determined for each source photon i as a function of its energy E_i . The MEAC ratios per photon are summed and, after the Monte Carlo calculation, divided by the total number of photons NP to get the average MEAC ratio for the spectrum. Finally, the PMMA dose is multiplied with the mean MEAC ratio to get the air dose in the cylindrical holes:

$$D_{\text{air}} = D_{\text{PMMA}} \cdot \frac{1}{\text{NP}} \sum_i \frac{\text{MEAC}_{\text{air}}(E_i)}{\text{MEAC}_{\text{PMMA}}(E_i)} \quad (7)$$

2.5. Validation of the bowtie filter model

2.5.1. Validation of the basic bowtie filter model. Although not to be used for a specific CT scanner, the basic bowtie filter model has to be checked with respect of its performance relative to the results for the so-called ‘perfect filter’. Monte Carlo calculations were carried out

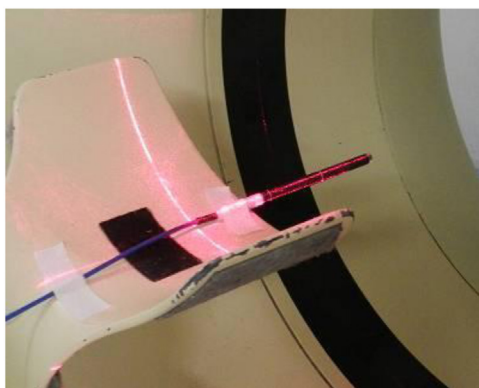


Figure 8. Pencil ionization chamber in free in air measuring position.

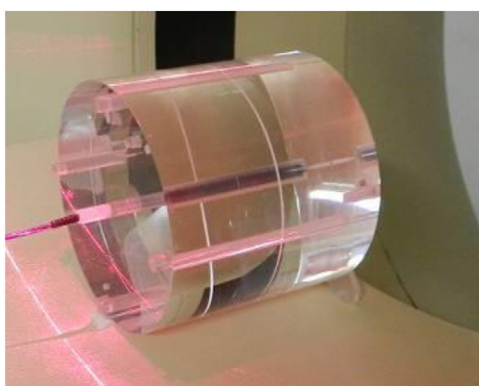


Figure 9. CTDI HEAD phantom with pencil ionization chamber in central hole.

for one single rotation with 1 cm beam collimation between 7 cm and 8 cm, i.e. at mid-length of the cylinder. The DSI was 54 cm, the fan angle 56° . A 120 kVp spectrum with 7° anode angle and 5 mm Al flat filter was used. 20 million photons were simulated. The cut-off energies were 150 keV and 2 keV for electrons and photons, respectively.

2.5.2. Validation of the scanner-specific bowtie filter model. CTDI results calculated with the scanner-specific bowtie filter model were validated against corresponding data

- (a) published by CTDosimetry (www.impactscan.org),
- (b) calculated with proprietary data for the Philips Brilliance 40 and 64 CT scanner, and
- (c) measured with a PHILIPS Brilliance 40 and 64 CT scanner.

As for the mathematical validation, x-ray spectra as well as information on the material composition and the exact shape of the bowtie filter for the CT scanner Brilliance 40 and 64 were kindly provided by the manufacturer PHILIPS under a non-disclosure agreement. Together with additional data available in the scanner manual, the exact bowtie filter was modelled using two sigmoid Boltzmann functions (equation (4)) and the linear attenuation coefficients for the original filter material.

Using physical PMMA HEAD and BODY phantoms (PTW Model T40027) and the PHILIPS Brilliance 64 scanner at the Instituto de Medicina Integral Prof Fernandes Figueira

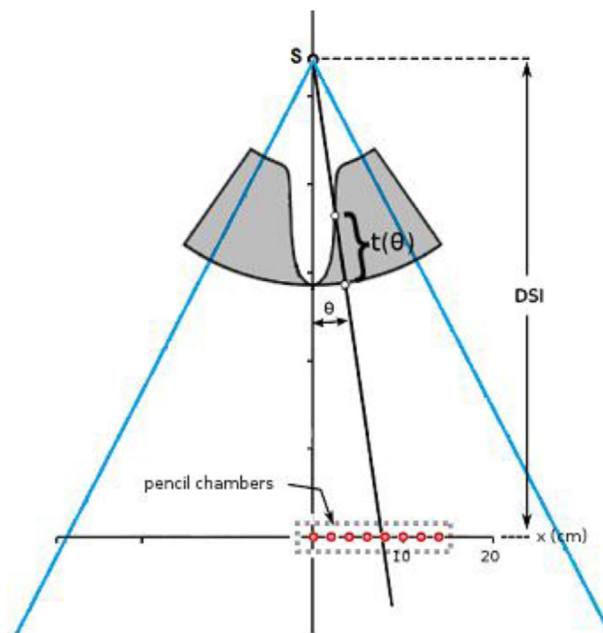


Figure 10. Exposure geometry for the measurement and the calculations of the lateral dose profiles including bowtie filter.

(IMIP) in Recife, Brazil, the following CTDIs were measured with a pencil ionization chamber (PTW, Model TW30009) made of PMMA coupled to an electrometer (PTW, Model Unidos E):

$CTDI_{100,a}$ free in air in the centre of rotation and at lateral positions, according to figure 8,

$CTDI_{100,c}$ in the central 10 cm hole and $CTDI_{100,p}$ in all four peripheral 10 cm holes of the PMMA phantoms, according to figure 9 for 80, 120 and 140 kVp, 200 mAs for a single rotation, 64 slices of 0.625 mm each (=4 cm scan length), pitch = 1. All measurement results were then normalized to a collimation of 1 cm, according to the definition of the CTDI quantities in section 2.1.

2.5.2.1. Validation using $CTDI_w/CTDI_{100,a}$. Using the data for ‘Air’, ‘centre’ and ‘perip’ (see table 1), ratios $CTDI_w/CTDI_{100,a}$, i.e. the weighted dose index normalized to the output of the x-ray tube, were initially calculated for all scanners listed by CTDosimetry. Then, 11 scanners, 4 from GE, 3 from SIEMENS, 3 from PHILIPS and 1 from TOSHIBA, were selected for comparison with corresponding ratios calculated with the scanner-specific bowtie filters of this study. Scanner-specific data, such as fan beam angle and DSI, were taken from the scanner manual or from scanner-specific information on www.impactscan.org. Calculations for a specific scanner always started with 120 kVp and $SFF = 1$. The collimation was always 1 cm at the centre of rotation. A initial value for the flat filter was defined based on information on the filtration in mm Al equivalent at 120 kVp provided by the scanner purchase reports to be found on www.impactscan.org. If the $CTDI_w/CTDI_{100,a}$ ratios of the calculation did not agree with the corresponding value from CTDosimetry, then the SFF was changed until the difference was less than 5%. This value for the SFF was then also used for all other tube potentials for that particular scanner. Sometimes, the initial flat filter was changed to improve agreement for tensions different from 120 kVp. Apart from the comparison with the CTDosimetry data,

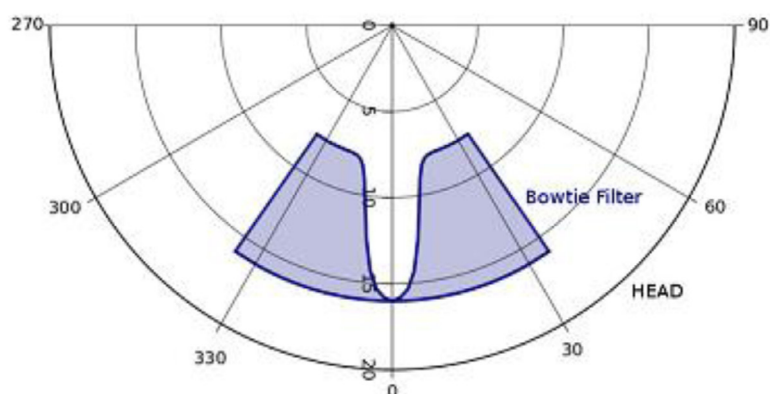


Figure 11. Basic PMMA bowtie filter for the HEAD phantom. Angular intervals are given in ($^{\circ}$), while the distances marked on the central ray represent (cm).

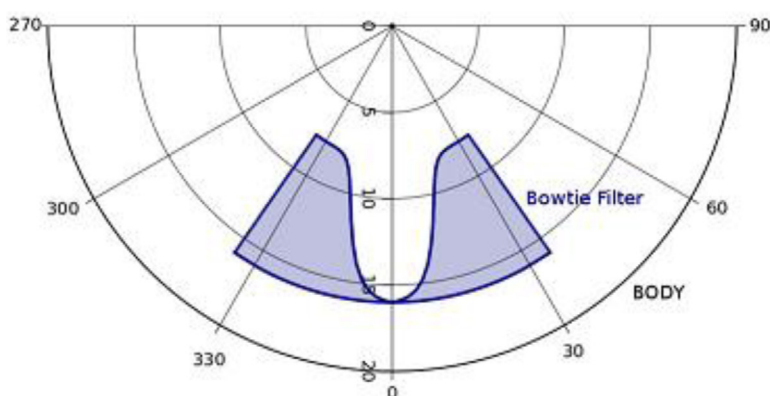


Figure 12. Basic PMMA bowtie filter for the BODY phantom. Angular intervals are given in ($^{\circ}$), while the distances marked on the central ray represent (cm).

additional comparisons were made for $CTDI_w/CTDI_{100,a}$ for the PHILIPS Brilliance 40 and 64 CT scanner between measurement and calculated data, i.e. $CTDI_w/CTDI_{100,a}$ for the pencil ionization chamber, for the scanner-specific bowtie filter and for the exactly modelled bowtie filter plus spectrum. The tube potential was 120 kV_p, the flat filter 8 mm Al, the fan beam angle = 56° , the DSI = 57 cm, collimation = 1 cm and pitch = 1.

2.5.2.2. Validation using $CTDI_{100,c}/100$ mAs, $CTDI_{100,p}/100$ mAs, and their ratio. Without changing the SFFs already determined in the previous section, $CTDI_{100,c}/100$ mAs, $CTDI_{100,p}/100$ mAs, and their ratios were compared with corresponding data of CT Dosimetry for the 4 scanners shown in table 1.

2.5.2.3. Validation using $CTDI_{100,a}$ in the centre and in lateral positions. According to figure 10, $CTDI_{100,a}$ was measured with a pencil ionization chamber on the axis of rotation and additionally in seven lateral positions with 2 cm intervals between them for 80, 120 and 140 kV_p, 200 mAs for a single rotation, 64 slices of 0.625 mm each (=4 cm scan length), pitch = 1. All measurement results were normalized to a collimation of 1 cm. Ratios between lateral

Table 4. CTDI_w/CTDI_{100,a} calculated from CTDosimetry data and by scanner-specific bowtie filter Monte Carlo calculations (UFPE). Also shown are the percentage differences, the values for the scanner filter factor (SFF), for the thickness of the flat filter and the DSI for the HEAD phantom for 11 CT scanners as a function of the tube potential. The average percentage difference is 0.89%.

Scanner	Tube potential (kVp)	HEAD phantom					
		CT dosimetry		Diff (%)	SFF	Flat Filter (mmAl)	DSI (cm)
		CTDI _w /CTDI _{100,a} (mGy/mGy)	UFPE				
GE Lightspeed Ultra	80	0.567	0.572	0.9	1.47	7	54.1
	100	0.614	0.614	0.0	1.47	7	
	120	0.641	0.641	0.0	1.47	8	
	140	0.658	0.649	1.4	1.47	8	
GE Lightspeed pro 16	80	0.544	0.558	2.5	1.60	7	54.1
	100	0.595	0.599	0.7	1.60	7	
	120	0.625	0.626	0.1	1.60	8	
	140	0.646	0.634	1.8	1.60	8	
GE Lightspeed RT	80	0.575	0.587	2.1	1.34	7	60.6
	100	0.625	0.631	0.9	1.34	7	
	120	0.657	0.658	0.2	1.34	8	
	140	0.676	0.669	1.0	1.34	9	
GE Lightspeed VCT	80	0.634	0.652	2.8	0.89	7	54.1
	100	0.688	0.696	1.1	0.89	7	
	120	0.723	0.723	0.0	0.89	8	
	140	0.740	0.730	1.3	0.89	8	
Philips Mx8000 IDT/Brilliance 16	90	0.778	0.767	1.4	0.46	8	57.0
	120	0.800	0.801	0.1	0.46	8	
	140	0.806	0.811	0.7	0.46	8	
Philips Big Bore	90	0.686	0.682	0.6	0.91	8	64.5
	120	0.718	0.718	0.0	0.91	8	
	140	0.726	0.725	0.1	0.91	8	
Philips Brilliance 64 or 40	80	0.735	0.710	3.3	0.63	8	57.0
	120	0.767	0.767	0.0	0.63	8	
	140	0.779	0.775	0.6	0.63	8	
Siemens Sensation 16	80	0.696	0.706	1.5	0.65	8	57.0
	100	0.744	0.745	0.1	0.65	8	
	120	0.762	0.763	0.1	0.65	8	
Siemens Sensation 64	80	0.686	0.684	0.3	0.77	8	57.0
	100	0.725	0.723	0.3	0.77	8	
	120	0.741	0.741	0.1	0.77	8	
Siemens Definition AS	80	0.614	0.635	3.4	1.15	9	59.5
	100	0.663	0.670	1.1	1.15	9	
	120	0.688	0.688	0.1	1.15	9	
	140	0.701	0.695	0.8	1.15	9	
Toshiba Aquilion 16	80	0.594	0.596	0.3	0.91	4	60.0
	100	0.663	0.665	0.2	0.91	5	
	120	0.717	0.718	0.2	0.91	8	
	135	0.751	0.733	2.4	0.91	10	

air kerma and air kerma in the centre were then compared to corresponding ratios calculated simultaneously for all chamber positions using a modified version of the Monte Carlo code mentioned above.

2.5.2.4. Validation using computational anthropomorphic phantoms. Additionally, proposed and exactly modelled bowtie filter results were compared for CT examinations using the anthropomorphic human phantoms MASH and FASH in supine posture (Cassola *et al* 2010). For the CT simulations the arms were removed and the phantoms were placed on a carbon fibre patient couch.

3. Results and discussion

3.1. Basic bowtie filters

The basic PMMA bowtie filter for the HEAD phantom is shown in figure 11 as a visualization of the function $t(\theta)$ given in equation (4), using the coefficients from table 2.

Table 3 presents the results as dose per air kerma at the iso-centre for the central and peripheral air volumes of the CTDI phantoms together with the statistical error. Columns 2 and 3 show the results without bowtie filter ($SFF = 0$, $W = 1$). The ratio between central and average peripheral dose is $0.0763/0.0935 = 0.816$, i.e. the distribution in the PMMA HEAD phantom is not homogeneous. Using the basic bowtie filter for the HEAD phantom ($SFF = 1$, $W = \exp[-\mu(E) \cdot t(\theta)]$) gives the data in columns 4 and 5. This time the ratio is $0.0692/0.0676 = 1.023$, i.e. close to the ideal value of 1.0. This indicates a homogeneous dose distribution in the CTDI HEAD phantom.

Figure 12 shows the basic bowtie BODY filter and Columns 6 and 7 of table 3 the corresponding results of the Monte Carlo calculation for the BODY phantom. Here, the ratio between central and average peripheral dose is $0.0216/0.0449 = 0.481$, close to the ideal value of 0.5. The results, both for the HEAD and the BODY phantoms, confirm that modelling the bowtie filters with sigmoid Boltzmann functions produces the desired dose distribution.

3.2. Scanner-specific bowtie filters

3.2.1. Validation using $CTDI_w/CTDI_{100,a}$

3.2.1.1. Comparison with CT Dosimetry. The results for these calculations are shown in tables 4 and 5 in the fourth column (UFPE) for the HEAD and the BODY phantom, respectively. The fifth column shows the percentage difference between the data from CT Dosimetry and from this study, which often was much smaller than 5%. Three iterations were necessary on average to get a good agreement. It may be noted that in table 4 for the HEAD phantom, only two cases show differences greater than 3% and the average difference is 0.89%. The statistical Monte Carlo error is 0.6%.

For the BODY phantom data in table 5, only three cases with percentage differences greater than 4% are seen. Here, the average difference is 1.64% and the statistical Monte Carlo error is 1.2%. These results indicate that the extension of the weight W by the scanner filter factor SFF leads to good results with regard to the adaption of the basic bowtie filters to specific scanners. Tables 4 and 5 also show the values for the SFF and the flat filter used for the adaptation to the $CTDI_w$ of the 11 scanners. The last column shows the DSI as given in the scanner manual.

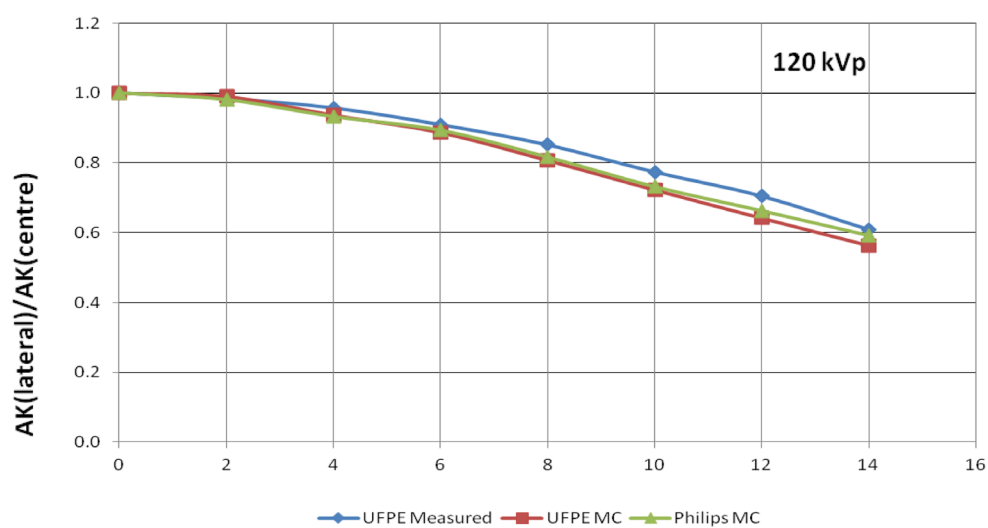


Figure 13. Relative lateral dose profiles, $AK(\text{lateral})/AK(\text{centre})$, free in air for 120 kVp using the Philips Brilliance 64 scanner: measured data (UFPE Measured), Monte Carlo data for the UFPE BODY bowtie filter (UFPE MC) and the original Philips bowtie filter and spectrum (Philips MC).

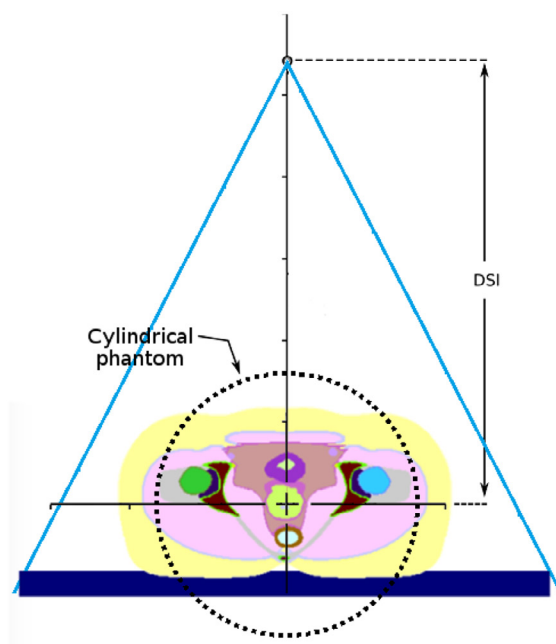


Figure 14. Abdomen CT/FASH phantom and CTDI BODY phantom.

The purpose of the iterative procedure is to approximate other dosimetric data; here those of CTDosimetry, but not to reproduce the real photon spectrum + flat filter of the scanner under consideration. This means, that the values for the flat filter shown in tables 4 and 5 are generally not those of the real spectrum which is proprietary.

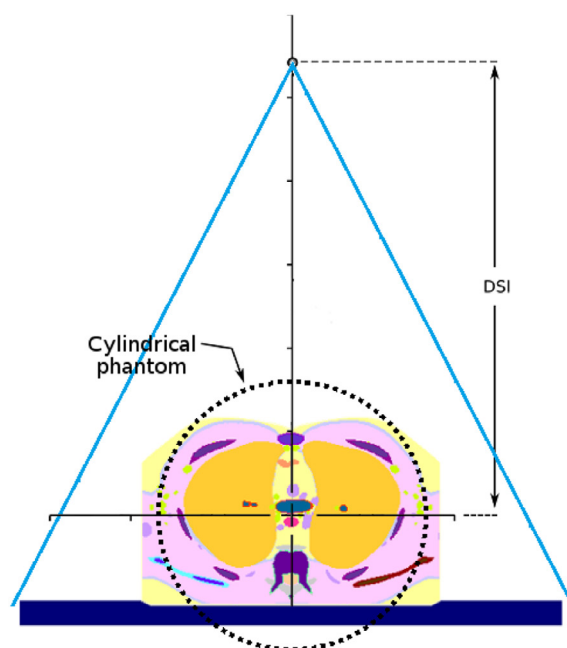


Figure 15. Thorax CT/MASH phantom and CTDI BODY phantom.

3.2.1.2. Comparison with measurements and calculations using proprietary data. Measurements of the central and peripheral $CTDI_{100}$ were made at 120 kVp in both phantoms, repeating each measurement three times. The results were normalized to 100 mAs. Table 6 shows the comparison between the manual-provided values and the measurements of this study. The average difference is 5%, with a maximum difference of 6.6%. Consequently, the performance of the measurement equipment can be considered satisfactory. It was felt necessary to check the equipment prior to the validation measurements.

Additional measurements of $CTDI_{100,c}$ and $CTDI_{100,p}$ were made for 80 and 140 kVp. All measurements were then compared with Monte Carlo data. Table 7 reports comparisons of $CTDI_w/CTDI_{100,a}$ ratios, i.e. the weighted CTDI index normalized to air kerma free in air on the axis of rotation. Shown are comparisons between Monte Carlo UFPE (results for the scanner-specific BODY and HEAD bowtie-filter), Monte Carlo PHILIPS (results for the exactly modelled bowtie filter and photon spectrum) and measured UFPE (results of the measurements with the PHILIPS Brilliance 64 scanner). The statistical errors of the Monte Carlo calculations were 0.6% and 1.3% for the HEAD and the BODY phantom, respectively. The measurement error was estimated to be around 3%.

In table 7, maximum and minimum percentage differences between the Monte Carlo results are 5.8% and 0.3%, respectively, with an average difference of 2.5%. The comparison between Monte Carlo UFPE and Measured UFPE show maximum and minimum percentage differences of 3.7% and 0%, respectively, with an average difference of 2.1%.

3.2.2. Validation using $CTDI_{100,c}/100$ mAs, $CTDI_{100,p}/100$ mAs, and their ratio. Table 8 shows $CTDI_{100,c}/100$ mAs (Centre), $CTDI_{100,p}/100$ mAs (Perip), and their ratio C/P for CTDosimetry and for UFPE for the four scanner mentioned in table 1. The UFPE data come from the same set of calculations which produced the data presented in tables 4 and 5, i.e. that SFFs and exposure parameters were not changed. The comparison between $CTDI_{100,c}/100$ mAs (Centre)

Table 5. $CTDI_w/CTDI_{100,a}$ calculated from CTDosimetry data and by scanner-specific bowtie filter Monte Carlo calculations (UFPE). Also shown are the percentage differences and the values for the scanner filter factor (SFF), the thickness of the flat filter and the DSI for the BODY phantom for 11 CT scanners as a function of the tube potential. The average percentage difference is 1.64%.

Scanner	Tube potential (kVp)	BODY phantom					
		CT dosimetry		Diff (%)	SFF	Flat filter (mm Al)	DSI (cm)
		$CTDI_w/CTDI_{100,a}$ (mGy/mGy)	UFPE				
GE Lightspeed Ultra	80	0.340	0.343	0.8	0.95	7	54.1
	100	0.368	0.376	2.3	0.95	7	
	120	0.397	0.396	0.3	0.95	8	
	140	0.393	0.402	2.4	0.95	8	
GE Lightspeed pro 16	80	0.330	0.335	1.6	1.17	10	54.1
	100	0.358	0.356	0.5	1.17	10	
	120	0.373	0.374	0.2	1.17	10	
	140	0.381	0.376	1.3	1.17	10	
GE Lightspeed RT	80	0.369	0.380	3.1	0.87	10	60.6
	100	0.398	0.405	1.7	0.87	10	
	120	0.415	0.416	0.3	0.87	10	
	140	0.425	0.423	0.5	0.87	10	
GE Lightspeed VCT	80	0.266	0.275	3.5	1.76	10	54.1
	100	0.296	0.300	1.2	1.76	10	
	120	0.317	0.317	0.0	1.76	10	
	140	0.331	0.318	3.8	1.76	10	
Philips Mx8000 IDT/Brilliance 16	90	0.383	0.376	1.9	0.90	8	57.0
	120	0.406	0.406	0.0	0.90	8	
	140	0.404	0.411	1.6	0.90	8	
Philips Big Bore	90	0.378	0.374	1.1	0.94	8	64.5
	120	0.401	0.401	0.1	0.94	8	
	140	0.414	0.403	2.5	0.94	8	
Philips Brilliance 64 or 40	80	0.349	0.346	0.8	1.01	8	57.0
	120	0.389	0.390	0.2	1.01	8	
	140	0.405	0.396	2.3	1.01	8	
Siemens Sensation 16	80	0.403	0.394	2.3	0.66	8	57.0
	100	0.406	0.422	3.9	0.66	8	
	120	0.447	0.448	0.1	0.66	8	
	140	0.453	0.455	0.3	0.66	8	
Siemens Sensation 64	80	0.303	0.315	4.0	1.27	8	57.0
	100	0.339	0.338	0.3	1.27	8	
	120	0.360	0.360	0.0	1.27	9	
	140	0.382	0.368	3.6	1.27	10	
Siemens Definition AS	80	0.281	0.293	4.1	1.57	9	59.5
	100	0.312	0.313	0.2	1.57	9	
	120	0.330	0.331	0.3	1.57	9	
	140	0.341	0.336	1.6	1.57	9	
Toshiba Aquilion 16	80	0.238	0.248	4.3	1.71	4	60.0
	100	0.282	0.292	3.4	1.71	6	
	120	0.312	0.312	0.1	1.71	8	
	135	0.339	0.324	4.5	1.71	10	

Table 6. Comparison of measured air kerma indices for the CTDI PMMA phantoms with data given in the scanner manual.

PHILIPS Brilliance 64, collimation: 1 cm, pitch = 1						
Tube	(mGy/100 mAs)		(%)	(mGy/100 mAs)		(%)
Potential	HEAD phantom			BODY phantom		
120 kV	Manual	Measured	Diff	Manual	Measured	Diff
CTDI _{100,c}	10.36	10.58	2.1	3.36	3.58	6.6
CTDI _{100,p}	11.24	11.85	5.4	6.76	7.15	5.8

Table 7. Comparison between CTDI_w/CTDI_{100,a} ratios calculated with scanner-specific bowtie filters, with an exactly modelled bowtie filter and measured with an ionization chamber.

PHILIPS Brilliance 64, collimation: 1 cm, pitch = 1, DSI = 57 cm						
Potential (kV)	HEAD CTDI _w /CTDI _{100,a}			BODY CTDI _w /CTDI _{100,a}		
	(Gy/Gy)			(Gy/Gy)		
	Monte Carlo		Measured	Monte Carlo		Measured
	UFPE	PHILIPS	UFPE	UFPE	PHILIPS	UFPE
80	0.710	0.694	0.692	0.346	0.327	0.347
120	0.767	0.769	0.748	0.390	0.377	0.390
140	0.775	0.782	0.747	0.396	0.387	0.411
	SFF = 0.63	SFF = 1		SFF = 1.01	SFF = 1	

and CTDI_{100,p}/100 mAs (Perip) for CTDosimetry and UFPE data show excellent agreement (Philips Brilliance 64, 80 kVp, Body phantom) as well as large differences (Toshiba Aquilion 16, 135 kVp, Body phantom). The average difference is 34.5%. A look at the C/P ratios shows that the differences decrease. Excellent agreement is seen for Philips Brilliance 64, 140 kVp, Body phantom and maximum difference of 28.6% for Toshiba Aquilion 16, 100 kVp, Body phantom. Average C/P differences are now down to 11.6% and 10.4% for Head and BODY phantoms, respectively. The C/P values for UFPE are on average closer to the ideal values, 1.0 (HEAD) and 0.5 (BODY) than those for CTDosimetry. Apart from the bowtie filter, also the spectra and flat filters are proprietary. Therefore, spectra and flat filters used in the matching process described in section 2.5.2.1 can be quite different from the real spectra and flat filters of the scanners to be considered. Consequently, CTDI_{100,c}/100 mAs (Centre), CTDI_{100,p}/100 mAs (Perip), and their ratio (C/P) compared in table 8 can show good or poor agreement.

The agreement between CTDosimetry and UFPE data in table 8 can be improved, of course, by initiating a new adaption process with the intention not to match CTDI_w/CTDI_{100,a} (shown in tables 4 and 5) but now to match CTDI_{100,c}/100 mAs and CTDI_{100,p}/100 mAs, which would lead to new SFFs.

The bowtie filter model proposed here was designed to use one SFF per phantom and per scanner based on the described matching process for CTDI_w/CTDI_{100,a} for the following reasons: First, in CT dosimetry the quantity of interest is the CTDI_w or CTDI_{vol}, which is frequently shown on the front panel of a CT scanner, and second it makes sense to use this quantity normalized to the tube output CTDI_{100,a} because it is less sensitive to differences between real and simulated spectra and flat filters compared to CTDI_{100,c}/100 mAs and CTDI_{100,p}/100 mAs and can be matched very closely as was shown in tables 4 and 5.

Table 8. CTDI_{100,c}/100 mAs (Centre), CTDI_{100,p}/100 mAs (Perip), and their ratio (C/P) calculated with scanner-specific bowtie filters and taken from CTDosimetry.

Scanner	kVp	HEAD						BODY					
		CTDI (mGy/100 mAs)						CTDI (mGy/100 mAs)					
		CTDosimetry			UFPE			CTDosimetry			UFPE		
		Centre	Perip	C/P	Centre	Perip	C/P	Centre	Perip	C/P	Centre	Perip	C/P
GE lightspeed ultra	80	7.7	8.2	0.94	6.0	5.6	1.07	1.8	4.5	0.40	1.6	4.4	0.36
GE lightspeed ultra	100	14.5	14.7	0.99	11.2	9.9	1.13	3.9	8.5	0.46	3.4	7.8	0.44
GE lightspeed ultra	120	22.5	22.3	1.01	15.5	13.4	1.16	7.0	13.8	0.50	5.2	10.5	0.50
GE lightspeed ultra	140	31.6	30.9	1.02	21.3	18.3	1.16	9.9	18.9	0.52	7.5	14.2	0.53
Philips brilliance 64 or 40	80	4.6	5.4	0.85	5.2	5.7	0.91	1.3	3.0	0.43	1.3	3.4	0.38
Philips brilliance 64 or 40	120	15.7	16.8	0.93	15.0	15.3	0.98	5.1	10.0	0.51	4.7	9.2	0.51
Philips brilliance 64 or 40	140	22.9	24.8	0.92	20.5	20.9	0.98	7.9	14.9	0.53	6.7	12.6	0.53
Siemens definition AS	80	3.3	3.6	0.93	4.0	3.9	1.03	0.9	2.0	0.44	1.0	2.2	0.45
Siemens definition AS	100	6.7	7.1	0.95	7.7	7.2	1.07	1.9	3.9	0.49	2.2	4.1	0.54
Siemens definition AS	120	11.3	11.8	0.96	12.0	11.0	1.09	3.5	6.6	0.53	3.6	6.4	0.56
Siemens definition AS	140	16.6	17.3	0.96	16.6	15.1	1.10	5.5	9.7	0.56	5.3	8.7	0.61
Toshiba aquilion 16	80	8.3	10.1	0.82	7.8	8.6	0.91	2.4	6.6	0.36	1.8	4.4	0.41
Toshiba aquilion 16	100	15.7	17.3	0.90	11.8	12.1	0.98	4.8	11.7	0.41	2.9	5.5	0.53
Toshiba aquilion 16	120	24.5	26.6	0.92	13.2	12.7	1.04	8.0	17.4	0.46	3.7	6.5	0.57
Toshiba aquilion 16	135	32.5	35.0	0.93	14.4	13.5	1.07	11.0	23.1	0.48	4.4	7.2	0.61
Average C/P				0.94			1.04			0.47			0.50

801

Table 9. Relative lateral dose profiles, AK(lateral)/AK(centre), free in air for 80, 120 and 140 kVp using the Philips Brilliance 64 scanner: Measured data (Measured UFPE), Monte Carlo data for the UFPE BODY bowtie filter (MC UFPE), the original Philips bowtie filter and spectrum (MC Philips).

Philips Brilliance 64, collimation: 1 cm, pitch = 1, DSI = 57 cm									
Position (cm)	80 kVp			120 kVp			140 kVp		
	AK(lateral)/AK(centre)			AK(lateral)/AK(centre)			AK(lateral)/AK(centre)		
	(Gy/Gy)			(Gy/Gy)			(Gy/Gy)		
	Measured	Monte Carlo		Measured	Monte Carlo		Measured	Monte Carlo	
	UFPE	UFPE	PHILIPS	UFPE	UFPE	PHILIPS	UFPE	UFPE	PHILIPS
0	1.000	1.000	1.000	1.000	1.000	1.000	1.000	1.000	1.000
2	0.991	0.982	0.966	0.984	0.991	0.981	0.990	0.991	0.984
4	0.957	0.926	0.902	0.957	0.937	0.932	0.966	0.937	0.930
6	0.904	0.864	0.837	0.909	0.887	0.893	0.920	0.886	0.878
8	0.833	0.780	0.761	0.851	0.807	0.816	0.864	0.815	0.826
10	0.752	0.689	0.687	0.773	0.722	0.731	0.800	0.727	0.742
12	0.675	0.607	0.607	0.704	0.641	0.662	0.714	0.653	0.670
14	0.591	0.533	0.539	0.608	0.562	0.591	0.610	0.572	0.608
SFF:		1.01	1.00		1.01	1.00		1.01	1.00

802

Table 10. FASH organ and tissue doses normalized to $CTDI_{vol}$ for a CT abdomen simulation with the PHILIPS Brilliance 64 scanner. ‘UFPE’ represents the bowtie filter and photon spectrum modelled with the method proposed here. ‘Philips’ represents the use of the bowtie filter and photon spectrum according to the data provided by the manufacturer. C.V. = coefficient of variance (statistical error).

FASH reference phantom supine		Bowtie filter and spectrum				Difference (%)
CT Abdomen	UFPE		Philips			
Philips Brilliance 64, 120 kVp	D/ $CTDI_{vol}$	C.V.	D/ $CTDI_{vol}$	C.V.		
Collimation: 4 cm	(Gy/Gy)	(%)	(Gy/Gy)	(%)		
Colon wall	1.484	0.24	1.424	0.24	4.04	
Breasts, glandular	0.412	0.55	0.403	0.55	2.18	
Kidneys	1.779	0.27	1.696	0.27	4.67	
Liver	1.562	0.13	1.498	0.14	4.10	
Lungs	0.296	0.33	0.285	0.34	3.72	
Muscle	0.494	0.07	0.482	0.07	2.43	
Pancreas	1.696	0.42	1.598	0.43	5.78	
Small intestine wall	1.430	0.20	1.361	0.21	4.83	
Skin (beam area)	1.471	0.19	1.481	0.19	-0.68	
Spleen	1.496	0.41	1.466	0.41	2.01	
Stomach wall	1.606	0.38	1.529	0.39	4.79	
Uterus	0.733	0.77	0.675	0.80	7.91	
Heart wall	0.295	0.67	0.274	0.69	7.12	
Lymphatic nodes	0.835	0.37	0.787	0.38	5.75	
Skeleton average	1.136	0.09	1.101	0.09	3.08	
Maximum rbm absorbed dose	1.207	0.33	1.124	0.34	6.88	
Maximum bsc absorbed dose	1.688	0.72	1.554	0.74	7.94	
Weighted fash dose	0.820	0.39	0.781	0.41	4.76	
Average difference:					4.52	

3.2.3. Validation using $CTDI_{100,a}$ in the centre and in lateral positions. For the exposure conditions used in table 7, a similar comparison was made for the lateral dose profiles, measured with the pencil ionization chamber, as well as calculated by Monte Carlo with the proposed bowtie filter and with the proprietary data received from Philips. Figure 10 shows the exposure geometry and figure 13 the dose profiles as air kerma at a lateral position (AK(lateral)) normalized to the air kerma at the centre (AK(centre)) for 120 kVp.

Excellent agreement can be seen between the Monte Carlo results, good agreement for both calculated data sets compared to the measured results. In figure 13, however, with increasing distance from the centre, the measured data are greater than the calculated ratios. The reason for this could be the difference between the exposure geometries of measurement and calculation mentioned at the end of section 2.2.1, i.e. that the assembly of 8 PMMA chambers at the same time in the Monte Carlo calculation could perhaps cause a shielding effect for the inner chambers when the beam comes from 90° (East) or 270° (West). As for the differences to be seen between the two calculations for larger lateral distances, we believe that this is due to the difference between the bowtie filter model, spectrum and flat filter proposed here and the model based on the proprietary data from Philips.

Table 9 presents the complete results for the free in air measurements and Monte Carlo calculations of the air kerma (AK) on the axis of rotation and for seven lateral positions using

Table 11. MASH organ and tissue doses normalized to $CTDI_{vol}$ for a CT thorax simulation with the PHILIPS Brilliance 64 scanner. ‘UFPE’ represents the bowtie filter and photon spectrum modelled with the method proposed here. ‘Philips’ represents the use of the bowtie filter and photon spectrum according to the data provided by the manufacturer. C.V. = coefficient of variance (statistical error).

MASH phantom supine CT Thorax	Bowtie filter and spectrum				Difference (%)
	UFPE		Philips		
Philips Brilliance 64, 120 kVp	D/ $CTDI_{vol}$	C.V.	D/ $CTDI_{vol}$	C.V.	
Collimation: 4 cm	(Gy/Gy)	(%)	(Gy/Gy)	(%)	
Kidneys	0.348	0.53	0.327	0.54	6.03
Liver	0.510	0.20	0.483	0.20	5.29
Lungs	1.460	0.13	1.398	0.13	4.25
Muscle	0.421	0.05	0.411	0.05	2.38
Oesophagus	1.374	0.73	1.295	0.75	5.75
Skin (beam area)	1.314	0.17	1.307	0.17	0.53
Spleen	0.554	0.59	0.526	0.60	5.05
Stomach wall	0.287	0.80	0.272	0.82	5.23
Thymus	1.505	0.87	1.437	0.88	4.52
Thyroid	2.139	0.85	2.077	0.86	2.90
Heart wall	1.473	0.25	1.398	0.26	5.09
Lymphatic nodes	0.707	0.33	0.690	0.33	2.40
Skeleton average	0.877	0.07	0.858	0.07	2.17
Maximum RBM absorbed dose	1.464	0.77	1.399	0.79	4.44
Weighted mash dose	0.665	0.32	0.642	0.34	3.46
Average difference:					3.97

the scanner Philips Brilliance 64. The data are given as ratios between the air kerma in a lateral position and in the centre. Again, the measurement errors were about 3% and the statistical Monte Carlo errors between 0.7 and 0.9%. Monte Carlo results for the UFPE bowtie filter and for the real Philips bowtie filter show excellent agreement: The maximum difference is 5.9% for position 14 cm for 140 kVp, while average differences are 1.6%, 1.7% and 2.0% for 80, 120 and 140 kVp, respectively. Comparison between UFPE and Philips Monte Carlo results on the one hand and measured data on the other hand show a maximum difference of 11.2% for position 12 cm for 80 kVp, while average differences are 6.7% and 8.1% for 80 kVp, 4.6% and 3.4% for 120 kVp, and 5.6% and 4.1% for 140 kVp.

3.2.4. Validation using computational anthropomorphic phantoms. CT examinations with the PHILIPS Brilliance 64 scanner for abdomen and thorax have been simulated with the supine adult human phantoms FASH and MASH, respectively. The calculations have been done with axial contiguous scans for the bowtie filter and photon spectrum as proposed in this study (‘UFPE’), and with the bowtie filter and photon spectrum based on the data provided by the manufacturer (‘Philips’). For the modelled bowtie filter the tube potential was 120 kVp, with 8 mm Al filtration. The fan was angle 56° for all calculations.

Figures 14 and 15 show the exposure scenarios for the FASH and the MASH phantom, respectively. The anatomical cross-sections represent the largest lateral body extension along the scan length of the examination. For comparison the circumference of the CTDI BODY

phantom is also shown in the images. With a fan angle of 56° , all parts of the human body and of the CTDI BODY phantom are covered by the beam.

The results are shown in tables 10 and 11 as organ and tissue absorbed doses D normalized to the volumetric CTDI_{vol} , $D/\text{CTDI}_{\text{vol}}$, which report data only for organs and tissue absorbed doses with a statistical error of less than 1%. The last column in both tables shows the percentage difference between 'UFPE' and 'Philips', which is always smaller than 8% and on average 4.52 and 3.97% for FASH and MASH, respectively.

4. Conclusion

In order to calculate organ and tissue doses for patients submitted to CT examinations, it is necessary to take the effect of bowtie filters into account. The motivation for this investigation emerged when it became clear that one should try to find a mathematical characterization of bowtie filters for Monte Carlo CT dosimetry independent from proprietary data provided by CT manufacturers and without having to do complicated and time consuming measurements. The method proposed here uses sigmoid Boltzmann functions to model the attenuation by bowtie filters for head and body CT procedures, which can be adapted to any specific CT scanner by adding a so-called scanner filter factor (SFF) which modifies the attenuation in order to match the calculated normalized weighted dose index, $\text{CTDI}_w/\text{CTDI}_{100,a}$, with corresponding data known for that particular scanner. Here, this information was taken from CTDosimetry (www.impactscan.org), but there are other sources available, like the work by Lee *et al* (2014), or measurements of the $\text{CTDI}_w/\text{CTDI}_{100,a}$ for a particular CT scanner can be made. $\text{CTDI}_w/\text{CTDI}_{100,a}$ was chosen as the primary quantity of interest for the matching process, because of the practical significance of the CTDI_w in CT dosimetry and because the normalization to air kerma in the centre of rotation $\text{CTDI}_{100,a}$ makes this quantity more robust with respect to difference between the real unknown spectra and flat filters and those assumed in the proposed model, compared to its proper components $\text{CTDI}_{100,c}/100$ mAs or $\text{CTDI}_{100,p}/100$ mAs.

The bowtie filter model proposed here was validated against calculated and measured data in terms of: $\text{CTDI}_w/\text{CTDI}_{100,a}$, $\text{CTDI}_{100,c}$, $\text{CTDI}_{100,p}$, for the CTDI PMMA phantoms, $\text{CTDI}_{100,a}$ free in air laterally across the fan beam and $D/\text{CTDI}_{\text{vol}}$ in organs and tissues of computational anthropomorphic phantoms. For the $\text{CTDI}_w/\text{CTDI}_{100,a}$, the results of the method proposed here deviated on average less than 2% from corresponding data of CTDosimetry (www.impactscan.org). For the Philips Brilliance 64 scanner, comparison with calculations using proprietary data and with measurements showed average differences for $\text{CTDI}_w/\text{CTDI}_{100,a}$ of 2.5% and 2.1%, respectively. For $(\text{CTDI}_{100,c}/100 \text{ mAs})/(\text{CTDI}_{100,p}/100 \text{ mAs})$ the agreement was still within a margin of about 11% on average. Lateral dose profiles showed excellent agreement between Monte Carlo data: About 2% on average between the proposed bowtie filter model and the exactly modelled bowtie filter. Compared with measured data the calculated results agreed on average within 5%. In addition, calculations with adult human phantoms using the mathematical bowtie filters on the one hand and the exactly modelled Philips bowtie filter on the other hand have shown good agreement, on average within 5%, between the two sets of organ and tissue doses.

The uncertainties involved in the proposed bowtie filter model are the statistical error of the Monte Carlo calculations, which was mostly around 1% or less, and the cumulative error of the measurements, which was estimated to be around 3%. If one assumes a total error of 5% for calculations and measurements combined, then one can see that many differences observed are located within the margin of error. Using the CTDI phantoms for

the bowtie filter design causes a certain limitation with respect to the emission angle of the source photons. For angles greater than θ_{limit} , the bowtie filter thickness is constant for all source photons. Depending on the design of the real bowtie filter of a specific scanner, this could lead to higher or lower doses in peripheral parts of a computational phantom in CT simulations or for dose profiles for larger lateral distances as seen for the measurements and calculations presented in section 3.2.2. Another limitation is the fact that the real x-ray spectrum and the flat filter of a specific scanner are usually not known. The flat filters for the proposed bowtie filter model are often changed as a function of the adjustment of CTDI quantities to the quantities to be matched. This could explain the differences for the comparison of $C/P = (\text{CTDI}_{100,c}/100 \text{ mAs})/(\text{CTDI}_{100,p}/100 \text{ mAs})$ with the corresponding data from CTdosimetry (www.impactscan.org). On the other hand, these limitations do not prevent the $\text{CTDI}_w/\text{CTDI}_{100,a}$, from agreeing within 2% on average with the data from CTdosimetry (www.impactscan.org), which actually was the main purpose of the matching procedure. Finally, a limitation also exists with respect to the CTDI concept, which has been questioned for CT scanners with high slice numbers, when the collimation starts to exceed the length of the ionization chamber (Boone 2007).

A comparison with the methods used by other investigators cited in the introduction is not possible on the same level. Their methods are focussed on the particular scanner under consideration and therefore possibly more accurate for that scanner. However, these methods imply sophisticated, time-consuming measurements and calculations, and access to a specific CT scanner in the first place. In contrast, the model proposed here, perhaps being sometimes less accurate, provides a bowtie filter simulation for any type of CT scanner as long as the $\text{CTDI}_w/\text{CTDI}_{100,a}$ and all exposure parameters necessary for a Monte Carlo simulation are known, without using proprietary data and/or requiring access to a specific scanner. The question is not which type of procedure is better; the question is whether the sophisticated method is doable and/or necessary. If the answer is no, then the bowtie filter model proposed here can be a useful alternative.

Acknowledgments

The authors would like to thank the Conselho Nacional de Desenvolvimento Científico e Tecnológico—CNPq for financial support for research project 312384/2014–9. Special thanks go to Peter Prinsen and Yoad Yagil from the company PHILIPS for providing the proprietary data for the bowtie filter of the Brilliance 40/64 scanners and to Dr Mirella Carneiro Arnaud Benevides Gadelha and Dr Valéria Di Biase from the IMIP for providing access to the Brilliance 64 CT scanner. The authors want to thank Professor John M Boone from the University of California for helpful information and advice he provided with respect to the issues discussed in this paper.

Annex

Inside the cylindrical holes, photon interactions were simulated in PMMA and, at the end of the Monte Carlo transport, the absorbed dose (=kerma) in PMMA was converted into kerma in air by multiplying the results with the ratio between the mass-energy absorption coefficient (MEAC) of air and PMMA, averaged over the photon spectrum used. This procedure used the mono-energetic MEAC from NIST (2015) and their ratios, shown in table A1, for the calculation of an average MEAC for the photon spectrum used for the Monte Carlo transport.

In order to verify this method, Monte Carlo calculations with the CTDI HEAD and BODY phantoms were made, first with air inside the cylindrical holes, simulating transport of 1.0×10^9 and 1.55×10^9 photons, respectively, and calculating the air kerma straightforward,

Table A1. Mass-energy absorption coefficients for air and PMMA as well as their ratio for photon energies between 1 and 200 keV (NIST 2015).

E (MeV)	AIR	PMMA	AIR/PMMA ratio
	μ_{en}/ρ (cm ² g ⁻¹)	μ_{en}/ρ (cm ² g ⁻¹)	
1.00×10^{-3}	3.60×10^3	2.79×10^3	1.29×10^0
1.50×10^{-3}	1.19×10^3	9.13×10^2	1.30×10^0
2.00×10^{-3}	5.26×10^2	4.02×10^2	1.31×10^0
3.00×10^{-3}	1.61×10^2	1.23×10^2	1.31×10^0
4.00×10^{-3}	7.64×10^1	5.18×10^1	1.47×10^0
5.00×10^{-3}	3.93×10^1	2.63×10^1	1.50×10^0
6.00×10^{-3}	2.27×10^1	1.50×10^1	1.52×10^0
8.00×10^{-3}	9.45×10^0	6.11×10^0	1.54×10^0
1.00×10^{-2}	4.74×10^0	3.03×10^0	1.57×10^0
1.50×10^{-2}	1.33×10^0	8.32×10^{-1}	1.60×10^0
2.00×10^{-2}	5.39×10^{-1}	3.33×10^{-1}	1.62×10^0
3.00×10^{-2}	1.54×10^{-1}	9.65×10^{-2}	1.59×10^0
4.00×10^{-2}	6.83×10^{-2}	4.60×10^{-2}	1.49×10^0
5.00×10^{-2}	4.10×10^{-2}	3.07×10^{-2}	1.34×10^0
6.00×10^{-2}	3.04×10^{-2}	2.53×10^{-2}	1.20×10^0
8.00×10^{-2}	2.41×10^{-2}	2.30×10^{-2}	1.05×10^0
1.00×10^{-1}	2.33×10^{-2}	2.37×10^{-2}	9.82×10^{-1}
1.50×10^{-1}	2.50×10^{-2}	2.66×10^{-2}	9.39×10^{-1}
2.00×10^{-1}	2.67×10^{-2}	2.87×10^{-2}	9.30×10^{-1}

Table A2. CSDA range of electrons in air (NIST 2015).

Electrons in air	
Energy (keV)	CSDA range (cm)
150	26.50
125	19.60
100	13.50
90	11.26
80	9.20
70	7.30
60	5.60
50	4.10
40	2.76
30	1.66
20	0.81

and second with PMMA inside the cylindrical holes, simulating transport of 2×10^7 photons, and additionally calculating and applying to the PMMA kerma an average MEAC for the photon spectrum.

As mentioned in section 2.3, the electron cut-off energy was set to 150 keV. The air holes in the CTDI phantoms are circular tubes with 8 mm diameter and 10 cm length. Secondary electrons, released in the air volume or entering the air volume from the surrounding PMMA, can travel in the air holes with any angle, including parallel to the longitudinal axis of the circular

Table A3. Ratios of $CTDI_w/CTDI_{100,a}$ for the CTDI HEAD and BODY phantoms for secondary electron cut-off energies of 150 and 50 keV. ‘PMMA’ represents the calculations using PMMA in the cylindrical holes and applying the correction with the MEA coefficients, while ‘AIR’ indicates the calculation using air in the cylindrical holes. C.V. = coefficient of variance (statistical error).

120 kVp		HEAD phantom		BODY phantom	
Medium in holes	E_{cut} (keV)	$CTDI_w/CTDI_{100,a}$ (Gy/Gy)	C.V. (%)	$CTDI_w/CTDI_{100,a}$ (Gy/Gy)	C.V. (%)
PMMA	150	0.679	0.60	0.391	1.20
	50	0.680	0.60	0.389	1.20
AIR	50	0.681	2.50	0.390	3.80

tubes. This raises the question if a cut-off energy of 150 keV can be justified. Table A2 shows that a 150 keV electron can travel 26.5 cm in air. A cut-off energy of 150 keV would prohibit the electron to deposit energy in air, especially if it would travel in the direction of the longitudinal tube axis. On the other hand one could argue that only a few electrons would have this direction due to the incident direction of the photon fan beam and impinging first on the CTDI phantom. A comprehensive study of the angular distribution of the secondary electrons and their energy deposition in air as a function of the initial electron energy is at least beyond the scope of this investigation. Instead, a comparison was made between $CTDI_w/CTDI_{100,a}$ calculated for electron cut-off energies of 150 and 50 keV. The results, presented in table A3, show that the correction with the MEA coefficients leads to the same results as the straightforward calculation in air, and that an electron cut-off energy of 150 keV can be used because its application leads to the same result as the use of 50 keV cut-off energy, for example.

References

- Atherton J V 1993 A Monte Carlo study of dose distributions and energy imparted in computed dosimetry phantoms *PhD Thesis* University of Florida, available at <http://ufdc.ufl.edu//AA00004733/00001>
- Bauhs J A, Vrieze T J, Primak A N, Bruesewitz M R and Mc Collough C H 2008 CT dosimetry: comparison of measurement techniques and devices *Radiographics* **28** 245–53
- Boone J M 2007 The trouble with $CTDI_{100}$ *Med. Phys.* **34** 1364–71
- Boone J M 2010 Method for evaluating bow tie filter angle-dependent attenuation in CT: theory and simulation results *Med. Phys.* **37** 40–48
- Bootsma G J, Verhaegen F and Jaffray D A 2011 The effects of compensator and imaging geometry on the distribution of x-ray scatter in CBCT *Med. Phys.* **38** 897–914
- Brenner D, Elliston C, Hall E and Berdon W 2001 Estimated risks of radiation-induced fatal cancer from pediatric CT *AJR Am. J. Roentgenol.* **176** 289–96
- Brenner D J and Hall E J 2007 Computed tomography—an increasing source of radiation exposure *New Engl. J. Med.* **357** 2277–84
- Cassola V F, Kramer R, Brayner C and Khoury H J 2010 Poster-specific phantoms representing female and male adults in Monte Carlo-based simulations for radiological protection *Phys. Med. Biol.* **55** 4399–430
- Cranley K, Gilmore B J, Fogarty G W A and Desponds L 1997 Catalogue of diagnostic x-ray spectra and other data *The Institute of Physics and Engineering in Medicine (IPeM) Report No. 78* electronic version prepared by D Sutton September 1997
- DeMarco J J, Cagnon C H, Cody D D, Stevens D M, McCollough C H, Zankl M, Angel E and McNitt-Gray M F 2007 Estimating radiation doses from multidetector CT using Monte Carlo simulations: effects of different voxelized patient models on magnitudes of organ and effective dose *Phys. Med. Biol.* **52** 2583–97
- Graham S A, Moseley D J, Siewerdsen J H and Jaffray D A 2007 Compensators for dose and scatter management in cone-beam computed tomography *Med. Phys.* **34** 2691–703

- Huda W and Atherton J V 1995 Energy imparted in computed tomography *Med. Phys.* **22** 1263–9
- IAEA International Atomic Energy Agency 2007 *Dosimetry in Diagnostic Radiology: an International Code of Practice (Technical Reports Series No. 457)* (Vienna: IAEA)
- ICRP 1996 *Conversion Coefficients for Use in Radiological Protection Against External Radiation (ICRP Publication 74. International Commission on Radiological Protection)* (Oxford: Pergamon)
- ICRP 2007 *Recommendations of the International Commission on Radiological Protection (ICRP Publication 103 Ann. ICRP 37 vol 2–3)* (Oxford: Elsevier)
- Jones D G and Shrimpton P C 1991 Survey of CT Practice in the UK, Part 3: Normalized Organ Doses Calculated using Monte Carlo Techniques, National Radiological Protection Board, NRPB-R250
- Jucius R A and Kambic G X 1977 Radiation dosimetry in computed tomography *Appl. Opt. Instrum. Eng. Med.* **127** 286–95
- Kontson K and Jennings R J 2015 Bowtie filters for dedicated breast CT: theory and computational implementation *Med. Phys.* **42** 1453–62
- Kramer R, Cassola V F, Khoury H J, Vieira J W, de Melo Lima V J and Robson Brown K 2010 FASH and MASH: female and male adult human phantoms based on polygon mesh surfaces: dosimetric calculations *Phys. Med. Biol.* **55** 163–89
- Lee C, Kim K P, Long D J and Bolch W E 2012 Organ doses for reference pediatric and adolescent patients undergoing computed tomography estimated by Monte Carlo simulation *Med. Phys.* **39** 2129–46
- Lee E, Lamart S, Littl M P and Lee C 2014 Database of normalized computed tomography dose index for retrospective CT dosimetry *J. Radiol. Prot.* **34** 363–88
- Li X, Samei E, Segars W P, Sturgeon G M, Colsher J G, Toncheva G, Yoshizumi T T and Frush D P 2011 Patient-specific radiation dose and cancer risk estimation in CT: part II. Application to patients *Med. Phys.* **38** 408–19
- Li X, Shi J Q, Zhang D, Singh S, Padole A, Otrakji A, Kalra M K, Xu X G and Liu B 2015a A new technique to characterize CT scanner bow-tie filter attenuation and applications in human cadaver dosimetry simulations *Med. Phys.* **42** 6274–82
- Li X, Morgan A G, Liptak C L, Muryn J S, Dong F F, Primak A N and Segars W P 2015b Adult abdomen-pelvis CT: does equilibrium dose-pitch product better account for the kVp dependence of organ dose than conventional CTDI? *Med. Phys.* **42** 6258–68
- Liu H, Gu J, Caracappa P F and Xu G 2010 Comparison of two types of adult phantoms in terms of organ doses from diagnostic CT procedures *Phys. Med. Biol.* **55** 1441–51
- Mail N, Moseley D J, Siewerdsen J H and Jaffray D A 2009 The influence of bowtie filtration on cone-beam CT image quality *Med. Phys.* **36** 22–32
- McKenney S E, Nosrati A, Gelskey D, Yang K, Huang S, Chen L and Boone J M 2011 Experimental validation of a method characterizing bow tie filters in CT Scanners using real-time dose probe *Med. Phys.* **38** 1406–15
- McMillan K, Bostani M, Cagnon C, Zankl M, Sepahdari A R and McNitt-Gray M 2014 Size-specific, scanner-independent organ dose estimates in contiguous axial and helical head CT examinations *Med. Phys.* **41** 121909
- McNitt-Gray M F 2002 AAPM/RSNA physics tutorial for residents: topics in CT, radiation dose in CT1 *RadioGraphics* **22** 1541–53
- NCRP 2009 Ionizing radiation exposure of the population of the United States *NCRP Report No. 160* National Council on Radiation Protection and Measurements, Bethesda, MD
- NIST National Institute of Standards 2015 Tables of x-ray mass attenuation coefficients and mass energy-absorption coefficients <http://www.nist.gov/pml/data/xraycoef/> accessed 10 April 2015
- Shope T B, Gagne R M and Johnson G C 1991 A method for describing the doses delivered by transmission x-ray computed tomography *Med. Phys.* **8** 488–95
- Tkaczyk J E, Du Y, Walter D, Wu X, Li J and Toth T 2004 Simulation of CT dose and contrast-to-noise as function of bowtie shape *Proc. SPIE* **5368** 403–10
- Turner A C, Zhang D, Kim H J, Cagnon C H, Angel E, Cody D D, Stevens D M, Primak A N, McCollough C H and McNitt-Gray M F 2009 A method to generate equivalent energy spectra and filtration models based on measurements for multidetector CT Monte Carlo dosimetry simulations *Med. Phys.* **36** 2154–64
- Whiting B R, Dohatcu A C, Evans J D, Polite D G and Williamson J F 2015 Technical note: measurements of bow tie profiles in CT scanners using radiochromic film *Med. Phys.* **42** 2908–14
- Whiting B R, Evans J D, Dohatcu A C, Williamson J F and Polite D G 2014 Measurements of bow tie profiles in CT scanners using a real-time dosimeter *Med. Phys.* **41** 101915